This is a repository copy of *Lithium-ion battery thermal runaway propagation prevention — predicting critical parameters considering uncertainty*.

White Rose Research Online URL for this paper:
https://eprints.whiterose.ac.uk/id/eprint/235280/

Version: Accepted Version

Article:
Bugryniec, P.J. orcid.org/0000-0003-3494-5646 and Brown, S.F. orcid.org/0000-0001-8229-8004 (2026) Lithium-ion battery thermal runaway propagation prevention — predicting critical parameters considering uncertainty. Journal of Energy Storage, 143. 119679. ISSN: 2352-152X

https://doi.org/10.1016/j.est.2025.119679

© 2025 The Authors. Except as otherwise noted, this author-accepted version of a journal article published in Journal of Energy Storage is made available via the University of Sheffield Research Publications and Copyright Policy under the terms of the Creative Commons Attribution 4.0 International License (CC-BY 4.0), which permits unrestricted use, distribution and reproduction in any medium, provided the original work is properly cited. To view a copy of this licence, visit http://creativecommons.org/licenses/by/4.0/

Reuse
This article is distributed under the terms of the Creative Commons Attribution (CC BY) licence. This licence allows you to distribute, remix, tweak, and build upon the work, even commercially, as long as you credit the authors for the original work. More information and the full terms of the licence here: https://creativecommons.org/licenses/

Takedown
If you consider content in White Rose Research Online to be in breach of UK law, please notify us by emailing eprints@whiterose.ac.uk including the URL of the record and the reason for the withdrawal request.

eprints@whiterose.ac.uk
https://eprints.whiterose.ac.uk/

Lithium-ion Battery Thermal Runaway Propagation Prevention – Predicting Critical Parameters Considering Uncertainty

Dr Peter J. Bugryniec[a], Prof Solomon F. Brown[a,*]

[a]*School of Chemical, Materials and Biological Engineering, University of Sheffield, Sheffield, S1 3JD, UK*

Abstract

Li-ion batteries (LIBs) are integral to modern society, driving the electrification of transport and supporting renewable energy generation to meet Net Zero. However, LIBs suffer from the potential to undergo thermal runaway (TR) which can lead to fire and explosions. Computational modelling of TR is essential to understanding its hazards, and to accurately quantify risks there is a need to account for the uncertainty in TR behaviour. To adequately predict the safe limits of battery operation we incorporate the stochasticity of thermo-physical and kinetic reaction parameters in module thermal runaway propagation (TRP) analysis. A 0-dimension heat transfer model for TRP predictions is validated against experimental findings. From this, Monte Carlo simulations are undertaken to determine the uncertainty in the predicted cell temperatures, times to cell TR and times to TRP. The critical heat dissipation coefficient to prevent TRP considering cell uncertainty was found to be 2.5 and 4.6 times larger for LFP and NMC stacks, respectively, compared to the scenario where cell uncertainty was not considered. For the LFP stack, the less severe TR events mean, in theory, that TRP can be prevented by heat pipe or submersion cooling thermal management systems. Without considering cell stochasticity there is a significant overestimate of TRP time and an underestimate of critical heat dissipation coefficient to prevent TRP. Hence, the predicted safe time for evacuation and appropriate thermal management methods are inaccurate. This work highlights the need to incorporate uncertainty in predictions of risk.

Keywords: Battery Safety, Battery Abuse, Stochastic Modelling, Statistical Analysis, Risk Assessment

Nomenclature

Roman symbols

T_{max}	Maximum cell temperature (°C)
t_{TRP}	TRP time between cell$_i$ to cell$_{i+1}$ (s)
t_{TR}	Time (absolute) to cell TR (s)

Abbreviations

*Corresponding author

Email address: s.f.brown@sheffield.ac.uk (Prof Solomon F. Brown)

$BESS$	Battery energy storage system (stationary applications)	LFP	Lithium iron phosphate
CoV	Coefficient of variation	LIB	Lithium ion (Li-ion) battery
EV	Electric vehicle (automotive)	NMC	Lithium nickel manganese cobalt oxide
IQR	Interquartile range	TR	Thermal runaway
ISC	Internal short circuit	TRP	Thermal runaway propagation

1. Introduction

Today Li-ion batteries (LIBs) are ubiquitous to automotive [1], marine [2], aviation [3] and stationary energy storage applications. With this increased adoption and use in safety-critical applications, specifically the aviation [4] and marine [5] sectors, understanding and preventing thermal runaway propagation (TRP) is paramount [6].

TRP is the cascading effect of cell-to-cell and module-to-module thermal runaway (TR) failure [6, 7]. TR is of great concern as it leads to extreme heat generation and the production of flammable gasses [8]. These gases lead to fire or, in confined scenarios, explosions. Further, due to the nature of LIBs, LIB fires are very difficult to extinguish, can burn for prolonged periods and reignite hours or possibly days later [9, 10].

Unfortunately, at a cell level, TR is always possible even with safety devices installed, due to the chemical potential of the cell materials, therefore maintaining system safety is only possible by preventing TRP [7]. Experimental and computational studies have investigated the use of different thermal management (cooling) and thermal barriers (insulation) to prevent TRP [6, 11]. Further, cell TR behaviour can be uncertain due to natural variations in materials and structural properties introduced through the manufacturing process. As such, it is important to consider the uncertainties in battery parameters and model assumptions in design optimisation, especially in safety-critical applications, to determine the probability of the most severe events and the practicality of mitigating them. Therefore, this work aims to determine the consequence of cell variability on the optimised battery design for TRP prevention.

The variation in TR severity (i.e. maximum temperature) and time to TR has been shown by several sources [e.g. 12–14] for cells of different chemistries under accelerated rate calorimetry (ARC), oven exposure and constant power heating. Further, the probability density of the heat output from the ejected dust/gases, ejected electrode winding and through the cell's surface have been calculated by Walker *et al.*, showing that the electrode winding and dust/gases carry away most of the heat [15]. The uncertainty in maximum temperature, heating rate and mass loss under ARC has been determined from a limited number of tests [16]. Thus highlighting the necessity to be able to incorporate uncertainty into predictions of cell and pack TR failure.

The sensitivity of cell TR to thermo-physical [17–19] and decomposition kinetic parameters [20] has been studied. From which, it has been shown that increasing the activation energy of the SEI reaction delays the onset of TR but does not prevent it [20]. It is found that TR severity is influenced most by internal short resistance ratio, cooling power, electrolyte combustion and the heat release from anode decomposition [17]. Further, the ability to maintain thermal safety is reduced with increased degradation and internal resistance [21]. Huang *et al.* [19] determined TR initiation and propagation are highly dependent on heat capacity and thermal contact. Applying a Gaussian Process surrogate model, Yeardly *et al.* [18] found that emissivity, followed by convection and conductivity properties, are most significant parameters regarding the variability of TR onset time and maximum TR temperature (when kinetic parameters not considered). For a module of prismatic cells, the thermal runaway process was most influenced by the "critical temperature" (the TR inducing temperature), while the specific heat capacity significantly influenced TR duration [19].

In our previous work on cylindrical cells, we show that when considering uncertainty in thermo-physical and kinetic parameters it is possible to predict the increase in failure probability with environmental temperature and also the resulting change in hazard level [22]. Further, for a large array of cylindrical cells, when random heat transfer coefficients are considered the propagation front deviates from the ideal path [23]. Using a probability distribution function for cell failure based on cell surface temperature (determined from experimental results) Zhai *et al.* predicted the TRP path and its likelihood considering different locations of initiating cells in a four-by-four pack of cylindrical cells [24]. Using a surrogate model, Zhang *et al.* [25] predict the uncertainty in maximum cell temperature, finding at 45% SOC the greatest uncertainty occurs. They further showed that if TR occurs in the first cell of a stack there then is a 90% chance of full TRP. Xia *et al.* [21] considered the uncertainty in the cell mass, cell internal resistance, ambient temperature and operating power within a TR model of a battery module. From this, they showed it is possible to predict the mean and standard deviation of both the critical ambient temperature and operating power for reducing the risk of TR.

It is important to consider the stochastic nature of cell parameters to enable predictions of uncertainty on time to TR, severity of TR, critical parameters to prevent TR(P) and propagation pathway. However, no work has considered the uncertainty in the kinetic parameters governing cell exothermic decomposition (alongside thermo-physical parameters) to predict the critical parameters to prevent TRP in modules or packs. This is evidently a crucial point to address considering that the kinetic parameters directly govern the TR behaviour of a Li-ion cell.

Carrying out statistical analysis studies, such as Monte Carlo simulations, on stochastic parameters to predict the uncertainty in outcomes requires many thousands of independent runs. As such, models need to be as computationally efficient as possible while still retaining accuracy, leading to lumped or 0-dimensional models being preferred.

Lumped thermal resistive network modelling is shown to be a useful method for simulating cell TR and TRP in battery modules [26–28] and packs [23, 29, 30]. These models have been used to study how battery parameters affect propagation severity, speed and direction; as well as how propagation can be prevented, but do not consider the effect of uncertainty on these predictions. Further, the lumped thermal runaway models can be coupled with electrochemical models or 3D computation fluid dynamics models to account for charge/discharge behaviour and vent-gas dispersion respectively.

This work, therefore, aims to understand the effect of exothermic decomposition uncertainty in Li-ion batteries on the variation of TRP behaviour. In doing so our objectives are to (1) incorporate, for the first time, uncertainty of thermo-physical and reaction kinetic parameters in a battery module (pack) simulation; (2) predict the probability and uncertainty to which critical parameters can prevent TRP; and (3) compare how the chemistry of a battery module affects these predictions. From this, we wish to highlight the importance of incorporating TR uncertainty in the evaluation of safety systems and the integral role it plays in supporting risk assessments of battery systems at any scale - such as determining the probability a thermal management system can prevent TRP or predicting the available time for evacuation.

2. Methodology

This work considers six NMC prismatic cells in series to form a cell stack representing experimental work by Feng *et al.* [26]. The model is validated against the experimental data, while the model is further used to study a similar LFP stack to allow a comparison of the two chemistries. The governing energy balance and heat generation terms of the cell model are presented in Section 2.1. These are incorporated into the thermal resistive network model representing the 6-cell stack described in Section 2.2. Abuse of the stack is by nail penetration of the first cell, as in Ref. [26], which is modelled by an additional heating term representing an internal short circuit (ISC) described in Section 2.1.4. The uncertainty analysis, considering the effects of cell variations on the predictions of significant TRP values (maximum cell temperature, time to TR and time to TRP) and the prevention of TRP, is discussed in Section 2.3.

2.1. Lumped Li-ion Cell Thermal Runaway Model

The governing theory for the thermal and decomposition behaviour of the cell model follows previous work [31, 32] and is described below.

Table 1: Cell physical parameters [33].

Description	**Symbol**	**Unit**	**Value**
Cell mass	M_{cell}	kg	0.72
Cell heat capacity	$C_{p,cell}$	J/kg/K	1100
Cell width, y direction	W_{cell}	m	0.1480
Cell height, z direction	H_{cell}	m	0.0913
Cell depth, x direction	D_{cell}	m	0.0265
Tab height	H_{tab}	m	0.0020
Tab width	W_{tab}	m	0.0265
Cell surface area, z direction	A_{xy}	m^2	$W_{cell}D_{cell}$
Cell surface area, y direction	A_{xz}	m^2	$D_{cell}H_{cell}$
Cell surface area, x direction	A_{zy}	m^2	$W_{cell}H_{cell}$
Tab surface area	A_{tab}	m^2	$H_{tab}W_{tab}$

2.1.1. Energy Balance

The energy balance, and therefore the cell temperature, is governed by:

$$\rho_{cell}C_{p,cell}V_{cell}\frac{dT}{dt} = Q_{conv} + Q_{rad} + Q_{decomp} \tag{1}$$

This assumes the temperature gradient within the cell negligible so the lumped heat capacity assumption holds. Here, ρ (kg/m^3) is the density of the cell and V_{cell} (m^3) is the volume of the cell. Hence, $\rho_{cell}V_{cell}$ is equivalent to the mass of the cell M_{cell} (kg). Further, C_p (J/kg/K) is the heat capacity of the cell, T (K) is the temperature of the cell, t (s) is time, while Q_{conv}, Q_{rad} and Q_{decomp} (J/s) are heat sources for convection, radiation and TR decomposition respectively. The physical parameters of the cell are given in Table 1.

2.1.2. Heat Sources

The radiation and convection heat transfer to/from the environment are governed by:

$$Q_{rad} = A_{cell}\varepsilon_{rad}\sigma_{rad}(T_{amb}^4 - T^4) \tag{2}$$

$$Q_{conv} = A_{cell}h_{conv}(T_{amb} - T) \tag{3}$$

where A_{cell} (m^2) is the surface area of the cell, T_{amb} (K) is the ambient temperature, ε_{rad} (unit-less) is the radiation efficiency coefficient, σ_{rad} (J/s/m^2/K^4) is the Stefan–Boltzmann constant and h_{conv} (J/s/m^2/K) is the natural convection coefficient.

The decomposition heat generation is the sum of four major exothermic reactions:

$$Q_{decomp} = Q_{sei} + Q_{ne} + Q_{pe} + Q_{ele} \tag{4}$$

The heat from the decomposition of the solid electrolyte interphase (Q_{sei}), negative-electrode/electrolyte reaction (Q_{ne}), positive-electrode/electrolyte reaction (Q_{pe}) and the decomposition of the electrolyte (Q_{ele}) are described as:

$$Q_{sei} = -m_{ne} h_{sei} \frac{dC_{sei}}{dt} \tag{5}$$

$$Q_{ne} = -m_{ne} h_{ne} \frac{dC_{ne}}{dt} \tag{6}$$

$$Q_{pe} = m_{pe} h_{pe} \frac{dC_{pe}}{dt} \tag{7}$$

$$Q_{ele} = -m_{ele} h_{ele} \frac{dC_{ele}}{dt} \tag{8}$$

where m_i (kg), h_i (J/kg) and C_i (unit-less) are the mass of reactant, enthalpy of reaction and fractional conversion of reactant i, respectively, where $i = sei, ne, pe, ele$.

2.1.3. Reaction Rates

The rate of decomposition of species C_i are given by:

$$\frac{dC_{sei}}{dt} = -A_{sei} \exp\left(-E_{a,sei}/R_{gas}T\right) C_{sei}^{n_{sei}} \tag{9}$$

$$\frac{dC_{ne}}{dt} = -A_{ne} \exp\left(-E_{a,ne}/R_{gas}T\right) C_{ne}^{n_{ne}} \exp\left(-t_{sei}/t_{sei0}\right) \tag{10}$$

$$\frac{dt_{sei}}{dt} = A_{ne} \exp\left(-E_{a,ne}/R_{gas}T\right) C_{ne}^{n_{ne}} \exp\left(-t_{sei}/t_{sei0}\right) \tag{11}$$

$$\frac{dC_{pe}}{dt} = A_{pe} \exp\left(-E_{a,pe}/R_{gas}T\right) C_{pe}^{n_{pe1}} (1 - C_{pe})^{n_{pe2}} \tag{12}$$

$$\frac{dC_{ele}}{dt} = -A_{ele} \exp\left(-E_{a,ele}/R_{gas}T\right) C_{ele}^{n_{ele}} \tag{13}$$

where A_i (1/s) is the frequency factor, $E_{a,i}$ (J) is the activation energy, R_{gas} (J/K) is the ideal gas-constant, t_{sei} and t_{sei0} are the non-dimensional thickness and initial thickness of the SEI, and n_i is a non-dimensional power term. The parameters for the reaction kinetics of Eqs. (5) to (13) are given in Table 2.

Table 2: Kinetic parameters for thermal runaway reactions [34]. Values for the LFP chemistry in brackets [35], positive-electrode/electrolyte reaction only, all other values same as NMC.

Description	**Symbol**	**Value**
Frequency factors (1/s)		
Solid electrolyte interphase	A_{sei}	1.67×10^{13}
Negative-electrode/electrolyte	A_{ne}	1.67×10^{12}
Positive-electrode/electrolyte	A_{pe}	6.67×10^{11} (2.00×10^{8})
Electrolyte decomposition*	A_{ele}	1.00×10^{13}
Electrochemical short circuit†	A_{ec}	1.67×10^{10}
Activation energies (J)		
Solid electrolyte interphase	$E_{a,sei}$	2.24×10^{-19}
Negative-electrode/electrolyte	$E_{a,ne}$	2.24×10^{-19}
Positive-electrode/electrolyte	$E_{a,pe}$	2.03×10^{-19} (3.62×10^{-19})
Electrolyte decomposition	$E_{a,ele}$	1.75×10^{-19}
Electrochemical short circuit†	$E_{a,ec}$	1.40×10^{-19}
Heats of Reaction (J/kg)		
Solid electrolyte interphase	H_{sei}	2.570×10^{5}
Negative-electrode/electrolyte	H_{ne}	1.714×10^{6}
Positive-electrode/electrolyte	H_{pe}	3.140×10^{5} (1.947×10^{5})
Electrolyte decomposition‡	H_{ele}	7.200×10^{5}
Initial value of dependent variables (-)		
Solid electrolyte interphase	$C_{sei,0}$	0.15
Negative-electrode/electrolyte	$C_{ne,0}$	0.75
Solid electrolyte interphase thickness	$t_{sei,0}$	0.033
Positive-electrode/electrolyte	$C_{pe,0}$	0.04
Electrolyte decomposition	$C_{ele,0}$	1
Mass content in cell (kg)		
Anode	m_c	0.13
Cathode	m_p	0.29
Electrolyte§	m_e	0.18
Reaction orders (-)		
Solid electrolyte interphase	n_{sei}	1
Negative-electrode/electrolyte	n_{ne}	1
Positive-electrode/electrolyte, 1	$n_{pe,1}$	1
Positive-electrode/electrolyte, 2	$n_{pe,2}$	1
Electrolyte decomposition	n_{ele}	1
Gas constant (J/K)	R_{gas}	1.38×10^{-23}

*Fit.

†From Jiang *et al.* [29].

‡Fit given the range of values from [26, 33].

§From Feng *et al.* [36].

2.1.4. Internal Short Circuit

The decomposition heat can be extended to include heat generated by ISC, Q_{short} [29]:

$$Q_{short} = -H_{ec}(1 - \eta - \gamma)\frac{d\text{SOC}}{dt} \tag{14}$$

where H_{ec} (J) is the total electrochemical energy stored within the cell, η is an efficiency factor representing the fraction of energy leaving via the venting process, while γ is a factor denoting the energy release due to nail penetration. The term H_{ec} is calculated by:

$$H_{ec} = C \cdot V \cdot 3600 \tag{15}$$

where C is the capacity (Ah) and V is the nominal voltage of the cell respectively.

The change in SOC is [29, 34]:

$$\frac{d\text{SOC}}{dt} = -A_{ec}(1 - C_{pe})C_{ne}\exp\left(-E_{a,ec}/R_{gas}T\right) + \left(\frac{dC_{pe}}{dt} + \frac{dC_{ne}}{dt}\right)\text{SOC} \tag{16}$$

where A_{ec} and $E_{a,ec}$ are the frequency factor and activation energy of the electrochemical reaction. Further, the second term on the right-hand side represents the consumption of the active material, while the process stops when the SOC term reaches zero. The change in SOC determines the rate of energy release from the short, and hence the rate of heat generation. The range of SOC determines the overall possible amount of energy that can be released, i.e. a larger initial SOC leads to greater heat of electrical short.

The first cell is initiated into TR by nail penetration. This is modelled by:

$$H_{nail} = \gamma H_{ec} \tag{17}$$

For the initiation cell γ is fit to experimental data [29] but is zero for all other cells. In the initiation cell the heat released is assumed to cause near instantaneous temperature rise. Hence, the temperature of the cell immediately at the time of penetration is [29]:

$$T_{trigger,0} = \frac{\gamma H_{ec}}{C_{p,cell}M_{cell}} + T_{int} \tag{18}$$

where T_{int} is the initial cell temperature. The parameters for the ISC heat generation are given in Table 3.

Table 3: Cell electrochemical and internal short circuit parameters [29].

Description	**Symbol**	**Unit**	**Value NMC**	**LFP***
Cell capacity	C	Ah	25	16.25
Cell voltage, nominal	V	V	3.7	3.2
Electrical energy	H_{ec}	J	Eq. (15)	
Initial SOC	SOC_0	-	1	
Efficiency factor, vent energy	η	-	0.12	
Efficiency factor, nail energy, Cell 1	γ	-	0.51	
Efficiency factor, nail energy, Cell 2-6	γ	-	0.00	

*The capacity of the LFP cell is assumed to be 65% of the NMC cell considering each have the same form factor.

2.2. Thermal Resistance Network Model of Li-ion Module

A thermal resistive network is used because of its computational efficiency allowing for relatively fast simulation times making it practical for uncertainty analysis. Under the electrical circuit analogy [37] the governing equation for the energy balance is given by Eq. (19), where C_{th} is the thermal capacitance of the object (J/K) derived from the heat capacity and mass (see Eq. (1)).

$$C_{th}\frac{dT}{dt} = \frac{T_{amb} - T}{R} \tag{19}$$

R is the thermal resistance (K/W) derived from the right hand side of Eq. (1) where:

$$Q = \frac{T_{amb} - T}{R} \tag{20}$$

The conductive resistance is derived from Fourier's law of conduction, Eq. (21). Equating Eq. (21) to Eq. (20) conductive resistance is determined and given by Eq. (22).

$$q_{condiction,1-2} = \frac{\lambda_{12} A_{12}(T_1 - T_2)}{\delta_{12}} \equiv \frac{T_1 - T_2}{R_{12}} \tag{21}$$

$$R = \frac{\delta_{12}}{\lambda_{12} A_{12}} = \frac{1}{h_{cond} A_{12}} \tag{22}$$

Where A_{12} (m^2) is the area of an object in a given direction *1→2* (which can be averaged if the area changes from one point to the other), δ_{12} (m) is the distance between walls and λ (W/m/K) is the thermal conductivity of the material. The resulting conductive heat transfer coefficient h_{cond} equates to λ_{12}/δ_{12}.

Newton's law of cooling defining convective heat transfer is given by Eq. (3) and can be equated to Eq. (20) such

that:

$$h_{conv}A_{surface}(T_{surface} - T_{fluid}) \equiv \frac{T_{surface} - T_{fluid}}{R_{conv}} \tag{23}$$

where h_{conv} (W/m^2/K) is the convection coefficient and A_{Surf} (m^2) is the surface area of a given face. From this the convective resistance, R_{conv}, is therefore:

$$R_{conv} = \frac{1}{h_{conv}A_{surf}} \tag{24}$$

For two objects touching, but where conduction does not occur, the contact resistance (R_{cont}) is given as:

$$R_{cont} = \frac{1}{h_{cont}A_{surf}} \tag{25}$$

where h_{cont} (W/m^2/K) is the contact heat transfer coefficient.

Stefan–Boltzmann and Kirchhoff's radiation laws for a grey body, Eq. (2) can be expanded:

$$\begin{aligned} Q_{rad,1-2} &= \varepsilon_1 \sigma A_1 \left(T_1^4 - T_2^4\right) \\ &= \varepsilon_1 \sigma A_1 \left(T_1^2 + T_2^2\right)(T_1 + T_2)(T_1 - T_2) = h_{rad}(T_1 - T_2) \end{aligned} \tag{26}$$

where the radiation heat transfer coefficient (h_{rad}) is defined as:

$$h_{rad} = \varepsilon_1 \sigma A_1 \left(T_1^2 + T_2^2\right)(T_1 + T_2) \tag{27}$$

Hence, radiative heat transfer can be expressed in resistive terms as:

$$Q_{12} = \frac{T_1 - T_2}{1/(h_{rad}A_1)} = \frac{T_1 - T_2}{R_{rad}} \tag{28}$$

and the radiative resistance is:

$$R_{rad} = \frac{1}{h_{rad}A_1} \tag{29}$$

Each of the cells in the stack, see Fig. 1, are denoted by a lumped thermal node (*yellow* dot) with a temperature T_{cell} governed by Eq. (19) with heat sources from Sections 2.1.2 and 2.1.4. Each cell (node) is connected to its neighbours through appropriate thermal resistances (R_i) to create the thermal resistance network. Each cell considers heat conduction from its lumped mass to is surface in each principle direction (x, y and z) through resistances R_x, R_y and R_z, as well as conduction via the cell tabs to neighbour cells through resistances R_{tab}, as shown in Fig. 1.

At a cell's top/bottom and front/back surfaces heat is transferred through convective R_{conv} and radiative R_{rad}

Table 4: Thermal resistance definitions and parameters.

Description	**Symbol**	**Parameter values to determine R_i**
Conductive resistance, Eq. (22)		
x-direction	R_x	$\delta = D_{cell}/2$; $\lambda = 0.15\,\mathrm{W/m/K}^*$
y-direction	R_y	$\delta = W_{cell}/2$; $\lambda = 30\,\mathrm{W/m/K}^*$
z-direction	R_z	$\delta = H_{cell}/2$; $\lambda = 30\,\mathrm{W/m/K}^*$
Tab connections†	R_{tab}	$\delta = 0.001\,\mathrm{m}$; $\lambda = 0.5\,\mathrm{W/m/K}$
Contact resistance between cells, Eq. (25)	R_{cont}	$h_c = 1000\,\mathrm{W/m^2/K}^*$
Resistance between cell and environment†, Eq. (24) and Eq. (29)	R_h	Convection: $h_{conv} = 20\,\mathrm{W/m^2/K}$§ Radiation: $\varepsilon = 0.04$, $\sigma = 5.670\,37 \times 10^{-8}\,\mathrm{W/m^2/K^4}$
Environment temperature	T_{amb}	25°C

*From Jiang *et al.* [29].

†Equivalent conduction parameters from Feng *et al.* [33].

§The convection coefficient is assumed to be the same in all directions.

resistances, combined into an overall resistance R_h. For the front surface of cell one and the back surface of cell six heat transfer is also by radiation and convection, see Fig. 1. For the cell surfaces touching a neighbouring cell surface heat transfer is through contact resistance R_{cont} as shown in Fig. 1.

The parameter values for the thermal resistances are given in Table 4. The thermal resistive network model is built in MATLAB® Simulink® and is presented in Figure S1 of the supplementary material.

2.3. Uncertainty Analysis

Uncertainty analysis of the stack TRP behaviour is determined through Monte Carlo methods. Random values for cell reaction parameters (M_{cell}, $C_{p,cell}$, A_i, $E_{a,i}$, H_i for $i = sei, ne, pe, ele, ec$) are generated assuming a normal distribution and no interdependence. The parameters are generated using MATLAB®'s *normrnd* function given a mean and standard deviation, where the mean is assumed to be the parameter values from Tables 1 and 2 and the standard deviation is equal to 1% of the mean (as in previous work [22]), i.e. a CoV of 1%. This value is based on the variation in measurable parameters, mass and dimensions, and applied to the kinetic parameters as there is a lack of data on the values of kinetic parameters by direct measurement to determine their CoV independently. Note the value of $T_{trigger,0}$ (Eq. (18)) is the same in all cases given a cell's chemistry as it is based on the "base" parameters of Tables 1 and 3.

The appropriate sample size (i.e. number of replicates) *N* for the Monte Carlo analysis is determined in the results, see Section 3. Further, the random parameters are determined such that for each run of the sample size N each of the six cells has random parameters representing the cell-to-cell differences within a given batch of manufactured cells.

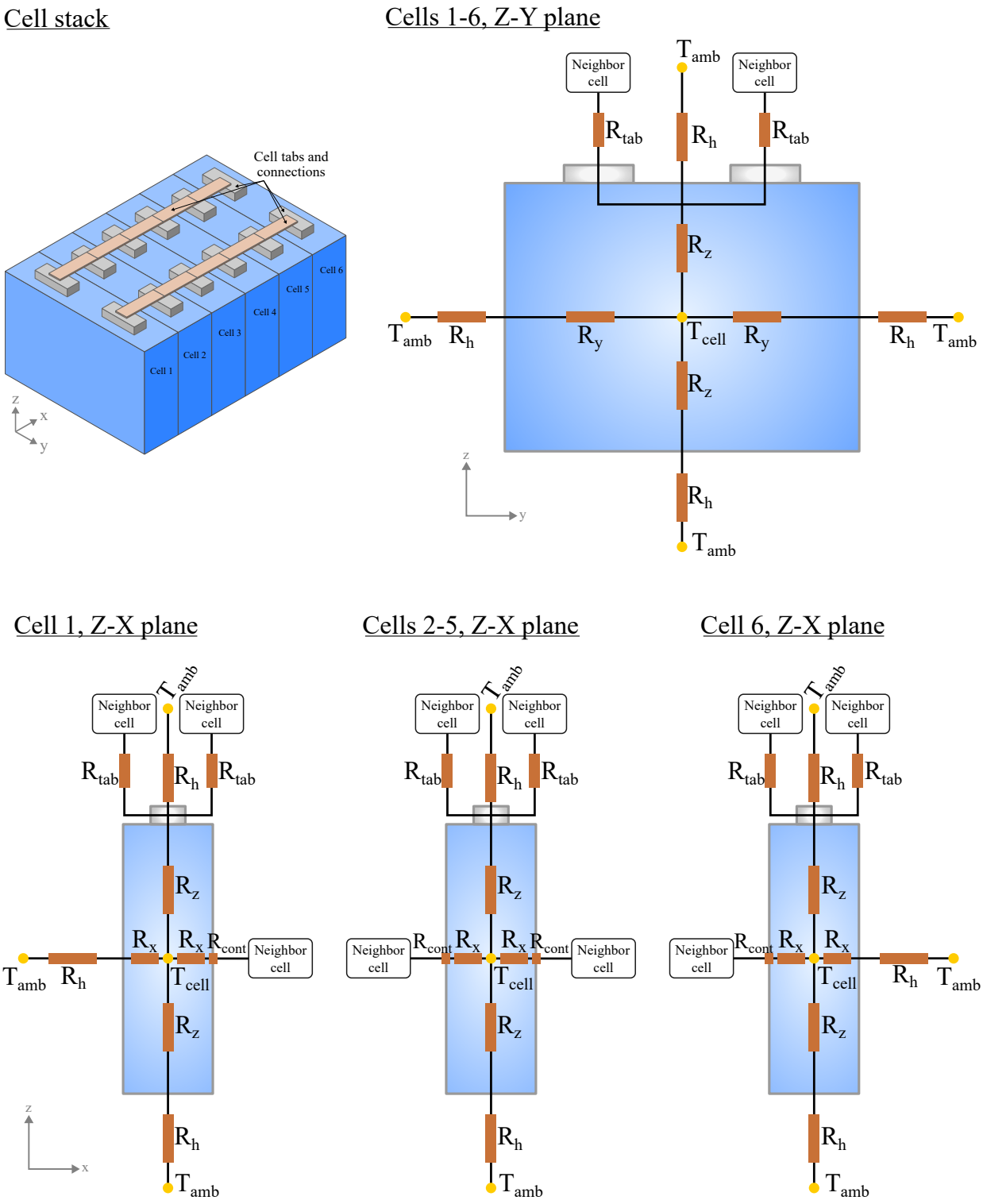

Figure 1: Schematic of battery stack and resistive network.

Lastly, each parameter generated within the normal distribution is checked to be positive as negative values have no real meaning.

Using this method the mean behaviour of TRP (with error quantified by a standard deviation) is predicted, i.e the maximum cell temperature, time to cell TR and time of cell TRP, and the median probability of preventing TRP (with error quantified as an interquartile range) is estimated. The mean is used in the analysis of TRP behaviour as the temperature and time are continuous numbers. The median is used in the analysis of the prevention of TRP because prevention is categorical, i.e. *yes/no* TRP has been prevented. The probability of prevention is determined from the percentage of "yes" in the sample size N, with the variation calculated from 100 samples (a.k.a 100 runs) each with a size N.

3. Results and Discussion

The TRP model of the 6-cell stack is first validated against experimental data, see Fig. 2(a). From this, it can be seen, for the NMC case, that the model predicts maximum cell temperatures and time to cell TR well. The errors in predicted maximum cell temperatures are shown in Table 5. The average error is approximately 5% when considering cells 2 to 6 (i.e. ignoring the initiation cell), and less than 5% when excluding cell 3 that shows a larger maximum temperature in the experimental data compared to the rest of the cells. While the simulated temperature profile to peak cell temperatures represents the experimental data well, the cooling of the cell after peak temperatures is slower. This is attributed to the thermal mass and heat capacity of the experimental cells decreasing after thermal runaway due to the venting process. This reduction leads to faster heat dissipation and, consequently, more rapid cooling of the experimental cells compared to the model, which currently does not account for venting. However, the critical parameters for TRP analysis, maximum cell temperature - T_{max}, the absolute time to cell TR - t_{TR} and the relative time between one cell undergoing TR following the previous cell (i.e the TRP time between cells) - t_{TRP}, are predicted well. As such, the model is deemed suitable for further studies.

Comparing the TRP predictions between the NMC (Fig. 2(a)) and LFP (Fig. 2(b)) cell stacks it can be seen that the LFP stack also undergoes TRP. However, the LFP stack has maximum cell temperatures 300°C to 350°C less than the NMC case while taking approximately twice as long to propagate from Cell 1 to 6. Note that according to Eq. (18), the instantaneous initiation temperatures (simulating nail penetration) are 179°C and 112°C for the NMC and LFP stack respectively. Even though the initiation temperature is much lower in the LFP case TR still occurs in Cell 1. Further, from Fig. 2 it is clear that TR initiates in both the NMC and LFP cells at a temperature much lower than 100°C as a rapid temperature rise is seen by this point.

Further details on the differences in T_{max}, t_{TR}, t_{TRP} for the two stacks of different chemistries are discussed in the next section. This is accompanied by a discussion of the effect of parameter uncertainty on model output (T_{max},

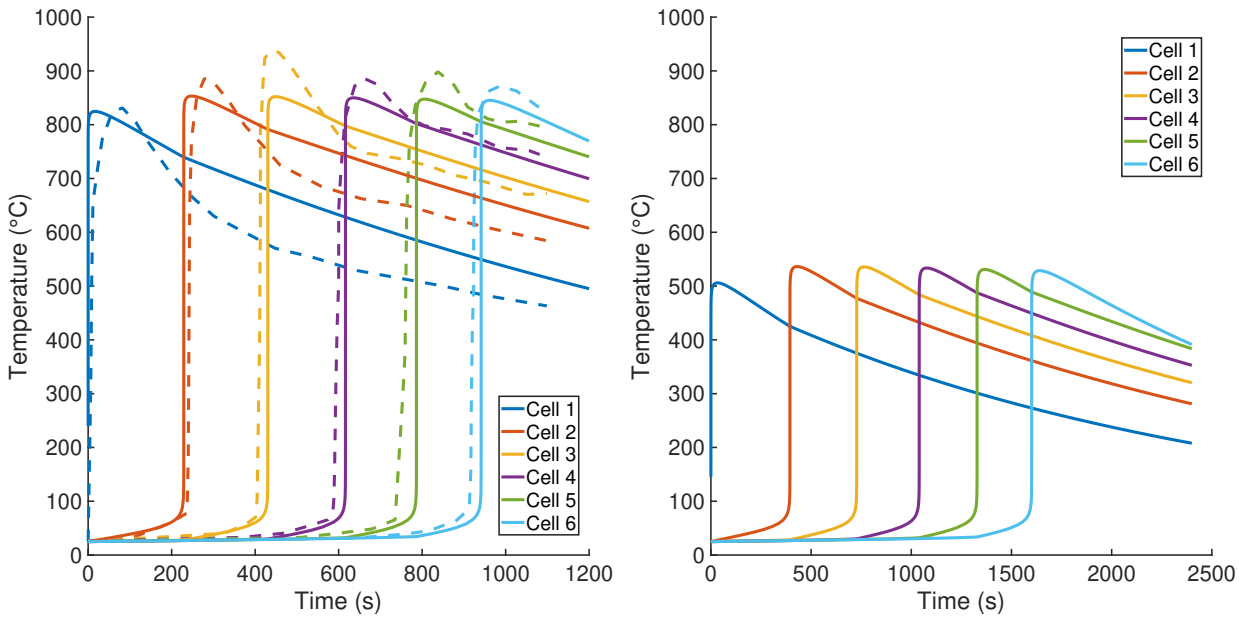

Figure 2: Predictions of TRP in a 6 cell stack (a) considering NMC cells, the simulation and experimental data is represented by solid and dashed lines respectively [experimental data from 26], and (b) considering LFP cells.

Table 5: Error in maximum cell temperature predictions of Fig. 2(a).

Cell	Error (%)
1	-0.8
2	-3.7
3	-9.1
4	-4.1
5	-5.7
6	-3.1

t_{TR}, t_{TRP}) uncertainty.

3.1. Thermal Runaway Propagation Analysis

To analyse the uncertainty in TRP behaviour, the effect of Monte Carlo sample size on results if first studied, see Fig. 3. From this, it can be seen that the error in mean maximum cell temperature (of Cell 6) is relatively unaffected by increased sample size. However, for the predicted time to TRP (for Cell 5 to Cell 6), the error significantly reduces to approximately 1% absolute error at $N = 10^3$. The CoV for both T_{max} and t_{TRP} initially increases with sample size but becomes stable at $N = 10^4$. Hence, considering the value of N at which the error no longer significantly reduces and where the CoV for T_{max} and t_{TRP} becomes stable, the smallest sample size that satisfies both conditions is $N = 10^4$. This used in the remainder of this section on the analysis of TRP uncertainty.

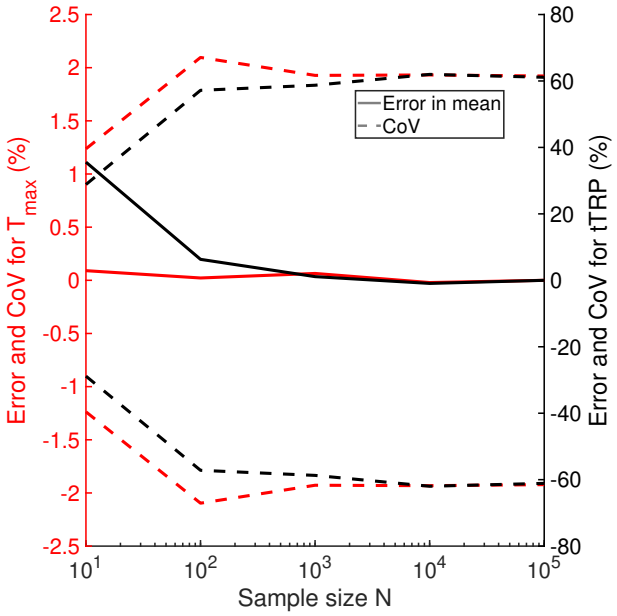

Figure 3: (Solid line) Error in the mean value of the maximum temperature of Cell 6 and the TRP time for Cell 5 to Cell 6 at different sample sizes, error calculated against the mean values at $N = 10^5$. (Dashed line) The coefficient of variation (CoV) at each sample size for the same cells.

Considering a sample size of $N = 10^4$, Fig. 4 presents the uncertainty in predictions of T_{max}, t_{TR}, t_{TRP} for the NMC cell and LFP cell stacks. Figs. 4(a) to 4(c) compare the Monte Carlo predictions to a base case simulation and experimental results for the NMC cell stack, and Figs. 4(d) to 4(f) compare the Monte Carlo predictions between the NMC cell and LFP cell stacks.

The predicted maximum temperature for the NMC stack (see Fig. 4(a)) is less than the experimental values (as noted in the discussion above) so direct comparisons to the Monte Carlo simulation can not be made. However, it can be seen that there is a slight downward trend in T_{max} as TR progresses through the stack. Further, it can be seen that there is a deviation of the mean value of the Monte Carlo simulation compared to the base case simulation, with the mean of the Monte Carlo simulation having lower values than the base case. Regarding t_{TR} and t_{TRP} in Fig. 4(b) and Fig. 4(c) it can be seen that the mean values are again slightly lower than the base case scenario. Most important is the t_{TRP}, which can be seen to reduce as propagation progresses. For the base case scenario, this behaviour is steady, while the experimental data follows a similar downward trend but with significant fluctuations. However, it can be seen from Fig. 4(c) that all the experimental t_{TRP} are picked up within one standard deviation of the mean values from the Monte Carlo simulation.

As shown above, even though T_{max} slightly reduces as TR progresses so does t_{TRP}. The reduction in t_{TRP} is attributed to the preheating of later cells by the TR of former cells [38–40]. Thus, applied to different module geometries or full packs the effect of failed cell location on the rate of TRP can be investigated. The above discussion

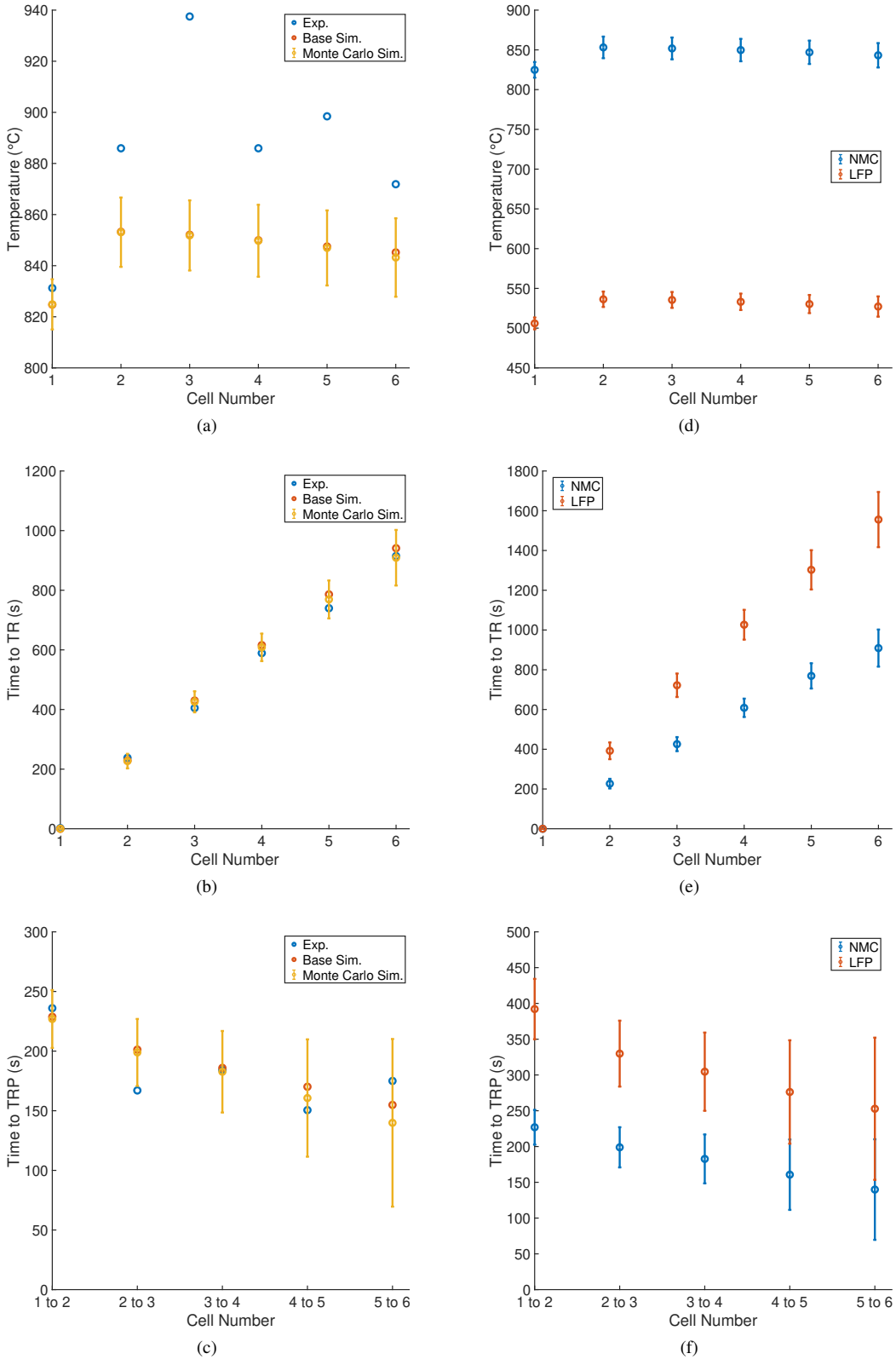

Figure 4: Uncertainty in predictions of T_{max} (a) and (d), t_{TR} (b) and (e), and t_{TRP} (c) and (f) for the NMC cell stack vs. experiential (a)-(c) and the NMC stack vs. the LFP stack (d)-(f). Error bars show +/- one standard deviation from mean.

Table 6: Coefficient of variation (CoV) in Figs. 4(d) to 4(f).

Cell	CoV (%) T_{max}		t_{TR}		t_{TRP}	
	NMC	LFP	NMC	LFP	NMC	LFP
1	1.19	1.43	N/A	N/A	N/A	N/A
2	1.59	1.80	10.70	10.75	10.70	10.75
3	1.61	1.83	8.28	8.18	14.11	14.00
4	1.66	1.94	7.58	7.30	18.70	17.94
5	1.73	2.15	8.26	7.58	30.62	26.16
6	1.82	2.42	10.25	8.91	50.25	39.30

also highlights the importance of considering cell variations to capture the fluctuation in maximum cell temperature and TRP time, and therefore the uncertainty in TRP behaviour.

Comparing the TRP behaviour of the NMC and LFP cell stacks (see Figs. 4(d) to 4(f)), it can be seen that the LFP stack behaves in much the same way as the NMC stack. Regarding maximum cell temperatures, the LFP stack reaches much lower peak cell temperatures (as also noted in Fig. 2). However, Fig. 4(d) and Table 6 show that as TRP progresses the uncertainty in the maximum cell temperature increases, with the LFP stack having greater uncertainty. The time to TR, see Fig. 4(e), is slower in the LFP cell stack but the CoV (Table 6) between to two chemistries is similar and shows no clear change with TRP progression. The TRP time, which reduces as propagation progresses, is greater for the LFP cell stack (see Fig. 4(e)). Further, as propagation progresses the uncertainty in t_{TRP} increases, see Fig. 4(e) and Table 6, while the NMC stack has a larger CoV at the latter stages of propagation.

Considering the CoV of the cell input parameters is 1%, we see this leads to 1.5-2.5 times more variation in T_{max} and an order of magnitude more variation in t_{TRP}. This shows that predictions on the time to TRP are much more sensitive than predictions of maximum temperature. This is attributed to the fact that some instances of cell-to-cell TRP time were negative, meaning that TRP was out of sequence, due to randomly generated parameters leading to cell stability being much lower than the former cell. Note that there is no correlation between maximum cell temperatures and time to cell TR.

The significant variation in t_{TRP} is important as it has practical implications on the predictions of safety at a pack and system level. Considering the requirement for a 5-minute warning of TR for EVs [41] or a similar minimum requirement for the propagation in BESSs, not accounting for cell variability could lead to considerable overestimation of TRP time. In turn, this would lead to incorrectly assessing a propagation event as acceptable when in many instances considering uncertainty it is not. Such is the importance of understanding cell TR variation and its incorporation into models for the prediction of events as pass/failure against safety criteria.

There is limited experimental data comparing NMC and LFP stacks, but our work broadly agrees with the tests

done by Schöeberl *et al.* [42]. The experimental comparison of NMC and LFP TRP uses larger capacity cells than this work, but the maximum cell temperatures are on average 900°C and 524°C for NMC and LFP respectively, compared to 845°C and 505°C predicted here. Further, the total time to complete TRP of the LFP stack is much longer than the NMC stack in both the simulated case and the experimental work of [42]. As such, this gives us further confidence in the simulation of the LFP stack. The t_{TRP} (cell-to-cell) of the experimental data shows greater propagation times for the LFP stack, similar to our predictions. However, while the LFP and NMC stacks show a downward trend in t_{TRP} as TRP progresses in our simulations and the experimental cases for NMC [26] and LFP [42], the NMC experimental case of [42] shows an upward trend. This highlights there is an uncertainty in t_{TRP} that needs to be considered in computational modelling.

3.2. Thermal Runaway Propagation Prevention

Predicting the variation of key TR metrics (i.e. T_{max}, t_{TR}, t_{TRP}) is important, but it is more insightful to understand how the same governing cell variations affect the values of critical parameters for TRP prevention. In this work, the necessary heat transfer conditions to prevent TRP are studied. To do this, the model is redefined such that convective and radiative heat transfer are considered together in one overall heat transfer coefficient h_{dis} (W/m^2/K). This allows for a simple method to determine the magnitude of heat transfer required to prevent TRP. The refined model is found to reproduce that of Fig. 2(a) when $h_{dis} = 25\,\mathrm{W/m^2/K}$ (which agrees with previous work by Feng *et al.* [26]), see Figure S2 in the supplementary material.

First, the value of h_{dis} required to prevent TRP is determined without considering cell variations to provide a point of reference. This is accomplished by running a parameter sweep of h_{dis} at 5 W/m^2/K steps whilst using a simulation time ten times greater than the base case ($t_{sim,base} = 1200\,\mathrm{s}$) to ensure all TR events are captured. The results of this are presented in Fig. 5. This shows that the NMC stack is prevented from full TRP at a value $h_{dis} = 335\,\mathrm{W/m^2/K}$ while TRP in the LFP stack is prevented at a value of $h_{dis} = 160\,\mathrm{W/m^2/K}$ (see Figure S3 in supplementary material for stack temperature profiles in the time domain). Similar magnitudes of heat dissipation have been shown in the literature, for a stack of five 3 Ah cells a convection heat transfer coefficient of $500\,\mathrm{W/m^2/K}$ is required to suppress TR [43].

As is expected from the LFP stack, due to the lower heat generation, it requires a lower h_{dis} than the NMC stack, but it is still a significant increase on $h_{dis} = 25\,\mathrm{W/m^2/K}$ that represents natural convection and radiation. Considering different heat dissipation methods, forced air cooling can reach up to 250 W/m^2/K, while heat pipes can reach 500 W/m^2/K and oil or water submersion cooling can reach 700 W/m^2/K and 1000 W/m^2/K respectively [26]. As such, the LFP stack could be managed with forced convection cooling while the NMC stack would require one of the alternate methods. Note, that one has to be conservative with these predictions as the additional heat sources from

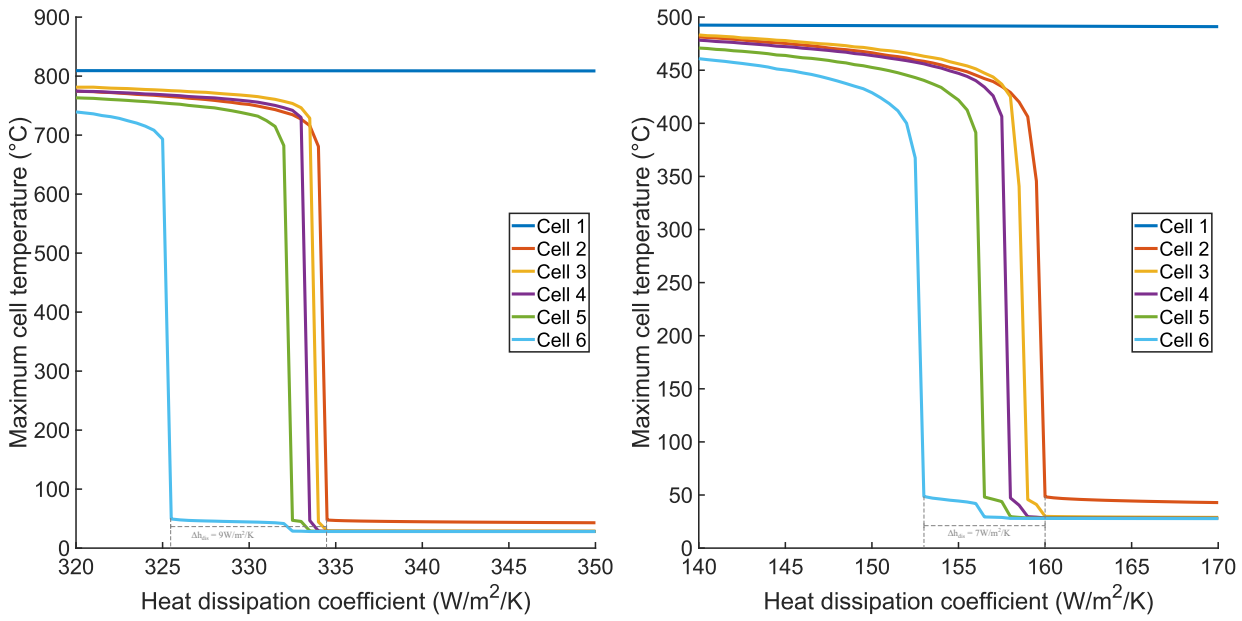

Figure 5: Parameter sweep of h_{dis} to determine critical value to fully prevent TRP, (a) NMC stack and (b) LFP stack.

electrochemical behaviour, cell series-parallel connectivity and fire are not considered here but have implications on TR and TRP behaviour in reality.

Following on from the base case scenario above, the effect of cell variation on the calculated value of h_{dis} for TRP prevention is studied. As TRP is a binary event, i.e. "yes/no TRP is prevented", the Monte Carlo simulation has to be sampled several times (with a given sample size) to calculate the variation in the predicted probability of preventing TRP. To determine an appropriate sample size for the study a sensitivity analysis is carried out.

The sensitivity analysis considers 100 samples (a.k.a runs) each with a sample size (i.e. number of replicates) N, again the simulation time is ten times the base case to ensure all TR events are captured. N is increased from 10^1 to 10^5, where at 10^5 the overall time for running the Monte Carlo simulation is prohibitive, thus 10^5 is taken as the scenario with maximum accuracy. The effect of N on the median and error (interquartile range - IQR and min/max range) is presented in Fig. 6. It can be seen that N has very little effect on the predicted median, but has a significant effect on the error. However, in relative terms, at a sample size of 10^4 the min/max values of the box plot are with 5% of the values at 10^5. As such the rest of the study uses 100 samples with a sample size of 10^4.

Under the Monte Carlo conditions described above, the probabilities of different severities of TRP (i.e. from full TRP to no TRP) are calculated for each stack at the h_{dis} determined in Fig. 5, as shown in Fig. 7. From this, it can be seen that for both chemistries complete TRP is only achieved in less than 50% of cases. This shows that a 1% CoV

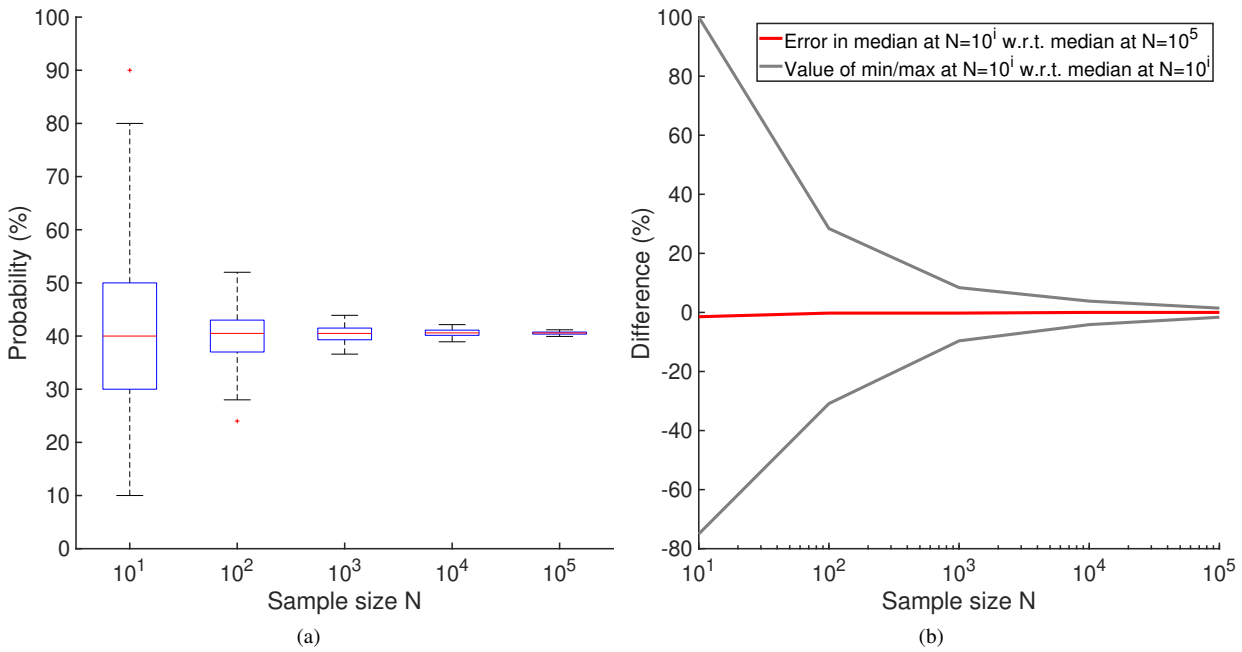

(a) (b)

Figure 6: Convergence of Monte Carlo simulations for 100 samples each with a sample size (or number of replicates) N. (a) Absolute values of predicted median and box plot data, and (b) values of predicted median relative to values at $N = 10^5$ and min/max data relative to median values at $N = 10^i$.

on cell kinetic and thermophysical parameters has a significant impact on determining pass/fail criteria. To further investigate this, a parameter sweep of h_{dis} now considering cell variability is undertaken.

Fig. 8 shows the parameter sweep of h_{dis} for one sample (with size $N = 10^4$) to approximately determine values of h_{dis} that lead to complete TRP prevention in 99% of cases. From this, it can be seen that the probability of the LFP stack being completely prevented from undergoing TRP increases more rapidly with h_{dis} than the NMC stack, while the NMC stack has a longer taper towards 100%. The LFP stack reaches a 99% percent probability at approximately $h_{dis} = 300\,\mathrm{W/m^2/K}$ while it is not until $h_{dis} = 850\,\mathrm{W/m^2/K}$ for the NMC stack. These values are used as a starting point to calculate the confidence in preventing TRP in more than 99.9% of cases (again using 100 samples with $N = 10^4$). For the NMC at $h_{dis} = 850\,\mathrm{W/m^2/K}$ the min/max values are not greater than 99%. As such, the uncertainty analysis on the NMC stack is carried out at values of h_{dis} at the maximum range of the study. This and similarly the LFP stack results are presented in Figs. 8(b) to 8(c).

From Fig. 8(b) it can be seen that at the maximum h_{dis} of the study (1550 W/m^2/K) the NMC stack is prevented from TRP in approximately 99.96% of cases, with a minimum value of 99.91%. At, $h_{dis} = 1500\,\mathrm{W/m^2/K}$ the minimum probability of prevention is 99.89%. However, the LFP stack (Fig. 8(c)) reaches a probability of preventing TRP in over 99.9% of cases (including the minimum percentage) at 400 W/m^2/K. Further, for the LFP stack with the relatively quick increase in median probability, there is a noticeable reduction in the IQR and min/max range of

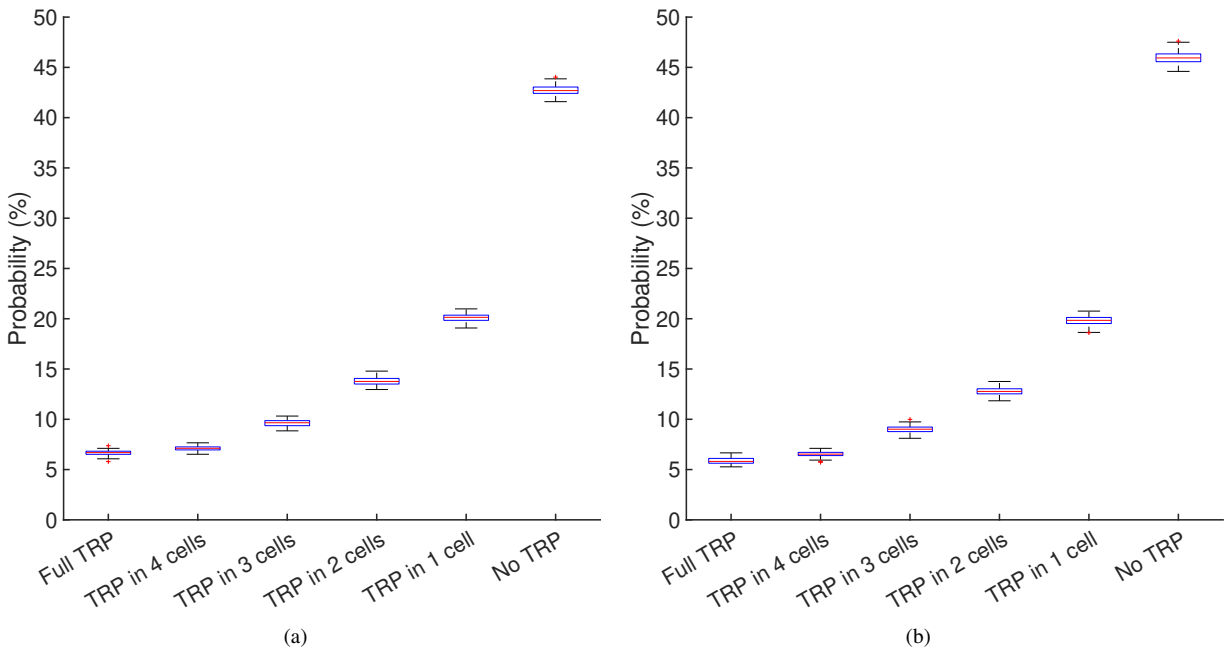

Figure 7: Probability of each level of TRP at h_{dis} determined in Fig. 5 for (a) NMC stack at $h_{dis} = 335\,\mathrm{W/m^2/K}$ and (b) LFP stack $h_{dis} = 160\,\mathrm{W/m^2/K}$.

the predicted probability. From this, it can be reasoned that even under the same cell variability (i.e. 1% CoV on input parameters) the greater severity of cell TR for the NMC chemistry leads to greater variation in the predicted probability of preventing TRP. Therefore, understanding and accounting for cell variability, while important, is more important in the NMC chemistry.

In comparison to the base case in which uncertainty is not considered (Fig. 5) the values of h_{dis} for the LFP and NMC stack are 2.5 and 4.6 times larger when considering uncertainty. This is a significant difference, which considering a safety-critical system would lead to devastating consequences. Preventing TRP in the LFP stack at $h_{dis} = 400\,\mathrm{W/m^2/K}$ is still theoretically possible with heat pipes or submersion cooling as long as the system can continually dissipate heat at this value and the working fluids can withstand the high temperatures. However, for the NMC stack, to achieve a h_{dis} value over 1550 W/m^2/K a system employing heat dissipation via liquid/vapour phase change is needed [44]. Using a lumped heat capacity model for the rapid undertaking of Monte Carlo simulations, as is common in system design and optimisation [45], we have shown that preventing TRP requires tailored cooling technologies specific to different battery chemistries. As such, future studies can use this method or findings to focus more detailed studies (accounting for dimensionality, fluid flow, etc.) on the most ideal cooling technology to determine specific operating parameters and more accurate overall heat transfer coefficients.

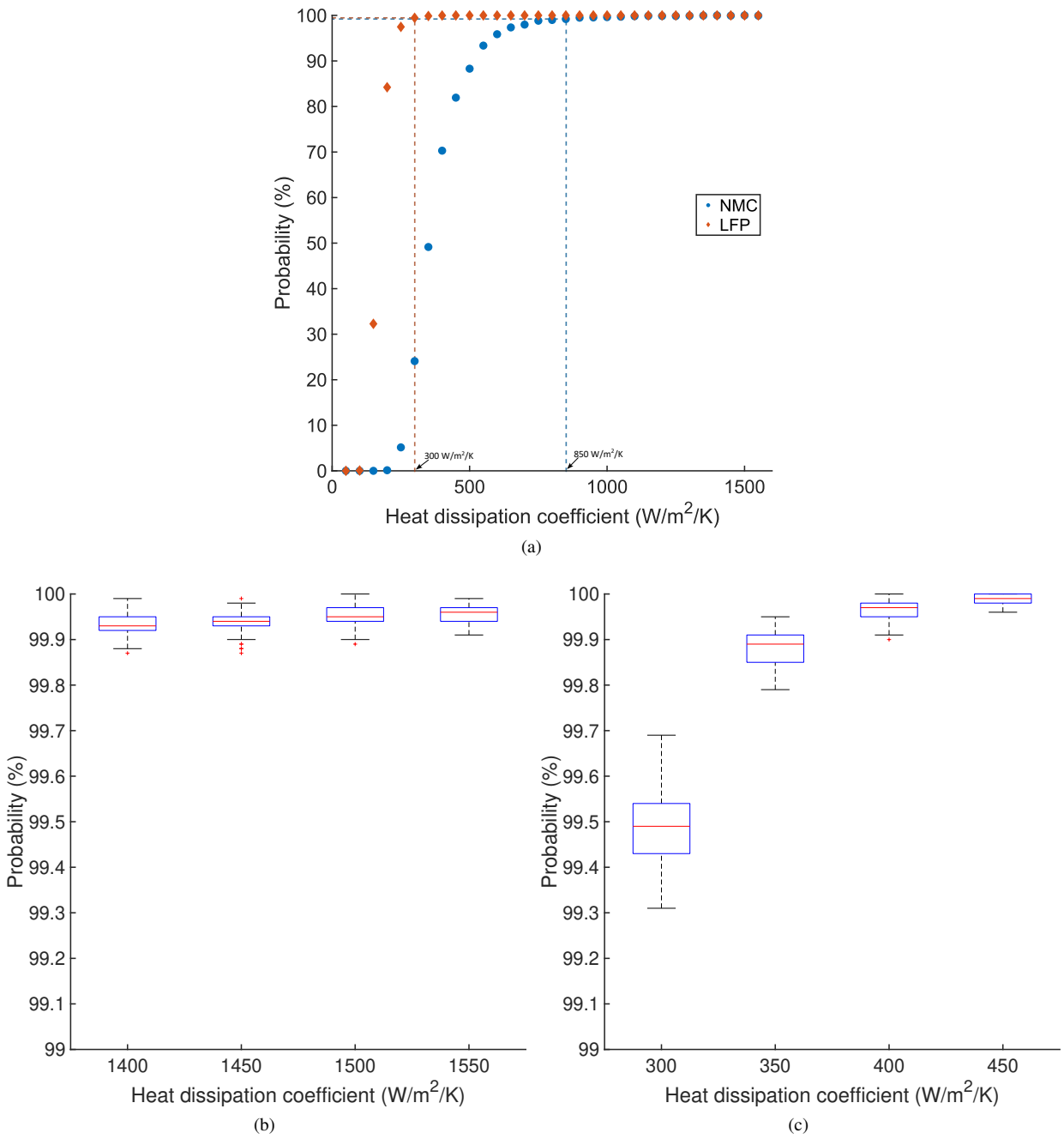

Figure 8: (a) Probability of fully preventing TRP at various h_{dis} values for NMC and LFP cells stacks (determined from 1 sample with a size of $N = 10^4$). (b) and (c) Certainty that TRP will be prevented for the (b) NMC stack and (c) LFP stack (determined from 100 sample with a size of $N = 10^4$).

4. Conclusions

A lumped heat capacity model of 6 prismatic cells is used to investigate the effect of cell-to-cell variations on TRP behaviour of NMC and LFP stacks. The variations in cell thermophysical and kinetic parameters are represented by normal distributions with a CoV of 1%. The model shows the LFP stack has cell temperatures 300°C to 350°C less than the NMC stack and propagation times approximately double that of the NMC stack.

For both chemistries, Monte Carlo simulations show that as TRP progresses maximum cell temperatures slightly reduce while there is a significant increase in cell-to-cell propagation speed. Further, as TRP progresses there is a slight increase in the uncertainty of predicted cell temperature, however, there is a significant increase in the uncertainty of cell-to-cell TRP time.

The critical heat dissipation coefficient to prevent TRP considering uncertainty is calculated to be $h_{dis} = 400\,\mathrm{W/m^2/K}$ for the LFP stack compared to $h_{dis} = 1550\,\mathrm{W/m^2/K}$ for the NMC stack. These values are 2.5 and 4.6 times larger, respectively, compared to the scenario where cell uncertainty is not considered.

From this, the key findings are:

1. the less severe TR events of LFP cells means, in theory, that TRP can be prevented by heat pipe or submersion cooling thermal management systems;

2. without considering cell uncertainty there could be a significant overestimation of the TRP time and hence available time for evacuation - putting people in harm's way; and

3. when not considering cell uncertainty the critical heat dissipation coefficient needed to prevent TRP is drastically underestimated, leading to incorrect assessments of safety and appropriate thermal management methods.

This work highlights the importance of accounting for uncertainty when predicting TRP behaviour so that the necessary propagation prevention method and available evacuation time can be correctly assessed, in turn allowing a more rigorous quantification of propagation risk. Further work is required to account for electrochemical behaviour to factor in the additional ohmic heat source during drive cycles, the effects of cell parallel/series connectivity, mass loss from venting and heat from off-gas fires in modules or batteries in a closed configuration or confined space. However, this work is integral to the battery sector to improve safety through facilitating probabilistic hazard assessments.

Conflicts of interest

There are no conflicts to declare.

Acknowledgements

This work was supported by the Faraday Institution [grant number FIRG061].

References

[1] Y. Ding, Z. P. Cano, A. Yu, J. Lu, Z. Chen, Automotive Li-Ion Batteries: Current Status and Future Perspectives, Electrochemical Energy Reviews 2 (1) (2019) 1–28. DOI:10.1007/s41918-018-0022-z.

[2] DNV, Marine Vessel Battery Statistics, online, accessed: 2023-11-28 (2023).

[3] A. Schwab, A. Thomas, J. Bennett, E. Robertson, S. Cary, Electrification of Aircraft: Challenges, Barriers, and Potential Impacts (10 2021). DOI:10.2172/1827628.

[4] S. Sripad, A. Bills, V. Viswanathan, A Review of Safety Considerations for Batteries in Aircraft with Electric Propulsion, MRS Bulletin 46 (5) (2021) 435–442. DOI:10.1557/s43577-021-00097-1.

[5] H. Helgesen, S. Henningsgård, A. A. Langli, Study on Electrical Energy Storage for Ships: Battery Systems For Maritime Applications – Technology, Sustainability And Safety, Tech. rep. (2020).

[6] S. Mallick, D. Gayen, Thermal Behaviour and Thermal Runaway Propagation in Lithium-ion Battery Systems – A Critical Review, Journal of Energy Storage 62 (2023) 106894. DOI:10.1016/j.est.2023.106894.

[7] X. Feng, D. Ren, X. He, M. Ouyang, Mitigating Thermal Runaway of Lithium-Ion Batteries, Joule 4 (4) (2020) 743–770. DOI:10.1016/j.joule.2020.02.010.

[8] P. J. Bugryniec, E. G. Resendiz, S. M. Nwophoke, S. Khanna, C. James, S. F. Brown, Review of Gas emissions from Lithium-ion Battery Thermal Runaway Failure — Considering Toxic and Flammable Compounds, Journal of Energy Storage 87 (2024) 111288. DOI:10.1016/j.est.2024.111288.

[9] L. B. Diaz, X. He, Z. Hu, F. Restuccia, M. Marinescu, J. V. Barreras, Y. Patel, G. Offer, G. Rein, Review - Meta-Review of Fire Safety of Lithium-Ion Batteries: Industry Challenges and Research Contributions, Journal of The Electrochemical Society 167 (9) (2020) 090559. DOI:10.1149/1945-7111/aba8b9.

[10] L. Zhang, K. Jin, J. Sun, Q. Wang, A Review of Fire-Extinguishing Agents and Fire Suppression Strategies for Lithium-Ion Batteries Fire, Fire Technology 60 (2) (2024) 817–858. DOI:10.1007/s10694-022-01278-3.

[11] S. Shahid, M. Agelin-Chaab, A Review of Thermal Runaway Prevention and Mitigation Strategies for Lithium-ion Batteries, Energy Conversion and Management: X 16 (2022) 100310. DOI:10.1016/j.ecmx.2022.100310.

[12] A. W. Golubkov, D. Fuchs, J. Wagner, H. Wiltsche, C. Stangl, G. Fauler, G. Voitic, A. Thaler, V. Hacker, Thermal-runaway experiments on consumer Li-ion batteries with metal-oxide and olivin-type cathodes, RSC Adv. 4 (2014) 3633–3642. DOI:10.1039/C3RA45748F.

[13] P. J. Bugryniec, J. N. Davidson, D. J. Cumming, S. F. Brown, Pursuing safer batteries: Thermal abuse of LiFePO4 cells, Journal of Power Sources 414 (2019) 557–568. DOI:10.1016/j.jpowsour.2019.01.013.

[14] L. Zhang, S. Yang, L. Liu, P. Zhao, Cell-to-cell variability in Li-ion battery thermal runaway: Experimental testing, statistical analysis, and kinetic modeling, Journal of Energy Storage 56 (2022) 106024. DOI:https://doi.org/10.1016/j.est.2022.106024.

[15] W. Q. Walker, G. A. Bayles, K. L. Johnson, R. P. Brown, D. Petrushenko, P. J. Hughes, D. T. Calderon, J. J. Darst, R. A. Hagen, B. A. Sakowski, J. P. Smith, K. I. Poast, E. C. Darcy, S. L. Rickman, Evaluation of Large-Format Lithium-Ion Cell Thermal Runaway Response Triggered by Nail Penetration using Novel Fractional Thermal Runaway Calorimetry and Gas Collection Methodology, Journal of The Electrochemical Society 169 (6) (2022) 060535. DOI:10.1149/1945-7111/ac7897.

[16] M. Buckwell, C. Kirchner-Burles, R. E. Owen, T. P. Neville, J. S. Weaving, D. J. Brett, P. R. Shearing, Failure and hazard characterisation of high-power lithium-ion cells via coupling accelerating rate calorimetry with in-line mass spectrometry, statistical and post-mortem analyses, Journal of Energy Storage 65 (2023) 107069. DOI:https://doi.org/10.1016/j.est.2023.107069.

[17] A. Kriston, A. Podias, I. Adanouj, A. Pfrang, Analysis of the Effect of Thermal Runaway Initiation Conditions on the Severity of Thermal Runaway—Numerical Simulation and Machine Learning Study, Journal of The Electrochemical Society 167 (9) (2020) 090555. DOI:10.1149/1945-7111/ab9b0b.

[18] A. S. Yeardley, P. J. Bugryniec, R. A. Milton, S. F. Brown, A study of the thermal runaway of lithium-ion batteries: A gaussian process based global sensitivity analysis, Journal of Power Sources 456 (2020) 228001. DOI:https://doi.org/10.1016/j.jpowsour.2020.228001.

[19] C. Huang, R. Bisschop, J. Anderson, A Sensitivity Study of a Thermal Propagation Model in an Automotive Battery Module, Fire Technology 59 (4) (2023) 1405–1420. DOI:10.1007/s10694-023-01383-x.

[20] K. Shah, A. Jain, Prediction of thermal runaway and thermal management requirements in cylindrical li-ion cells in realistic scenarios, International Journal of Energy Research 43 (5) (2019) 1827–1838. DOI:https://doi.org/10.1002/er.4411.

[21] Q. Xia, Y. Ren, Z. Wang, D. Yang, P. Yan, Z. Wu, B. Sun, Q. Feng, C. Qian, Safety risk assessment method for thermal abuse of lithium-ion battery pack based on multiphysics simulation and improved bisection method, Energy 264 (2023) 126228. DOI:https://doi.org/10.1016/j.energy.2022.126228.

[22] P. J. Bugryniec, S. F. Brown, Predictive hazard level assessment of Li-ion cell thermal runaway failure, in: Energy Storage Conference 2023 (ESC 2023), Vol. 2023, 2023, pp. 9–14. DOI:10.1049/icp.2023.3096.

[23] Y. Jia, M. Uddin, Y. Li, J. Xu, Thermal runaway propagation behavior within 18,650 lithium-ion battery packs: A modeling study, Journal of Energy Storage 31 (2020) 101668. DOI:https://doi.org/10.1016/j.est.2020.101668.

[24] H. Zhai, H. Li, P. Ping, Z. Huang, Q. Wang, An experimental-based Domino prediction model of thermal runaway propagation in 18,650 lithium-ion battery modules, International Journal of Heat and Mass Transfer 181 (2021) 122024. DOI:https://doi.org/10.1016/j.ijheatmasstransfer.2021.122024.

[25] W. Zhang, J. Yuan, J. Huang, Y. Xie, Uncertainty assessment method for thermal runaway propagation of lithium-ion battery pack, Applied Thermal Engineering 238 (2024) 121946. DOI:https://doi.org/10.1016/j.applthermaleng.2023.121946.

[26] X. Feng, X. He, M. Ouyang, L. Lu, P. Wu, C. Kulp, S. Prasser, Thermal Runaway Propagation Model for Designing a Safer Battery Pack with 25Ah $LiNi_xCo_yMn_zO_2$ Large Format Lithium Ion Battery, Applied Energy 154 (2015) 74–91. DOI:10.1016/j.apenergy.2015.04.118.

[27] J. Chen, D. Ren, H. Hsu, L. Wang, X. He, C. Zhang, X. Feng, M. Ouyang, Investigating the thermal runaway features of lithium-ion batteries using a thermal resistance network model, Applied Energy 295 (2021) 117038. DOI:https://doi.org/10.1016/j.apenergy.2021.117038.

[28] G. Wang, D. Kong, P. Ping, X. He, H. Lv, H. Zhao, W. Hong, Modeling venting behavior of lithium-ion batteries during thermal runaway propagation by coupling cfd and thermal resistance network, Applied Energy 334 (2023) 120660. DOI:https://doi.org/10.1016/j.apenergy.2023.120660.

[29] Z. Jiang, Z. Qu, J. Zhang, Z. Rao, Rapid Prediction Method for Thermal Runaway Propagation in Battery Pack Based on Lumped Thermal Resistance Network and Electric Circuit Analogy, Applied Energy 268 (2020) 115007. DOI:10.1016/j.apenergy.2020.115007.

[30] C. Xu, H. Wang, F. Jiang, X. Feng, L. Lu, C. Jin, F. Zhang, W. Huang, M. Zhang, M. Ouyang, Modelling of

thermal runaway propagation in lithium-ion battery pack using reduced-order model, Energy 268 (2023) 126646. DOI:https://doi.org/10.1016/j.energy.2023.126646.

[31] G.-H. Kim, A. Pesaran, R. Spotnitz, A Three-Dimensional Thermal Abuse Model for Lithium-ion Cells, Journal of Power Sources 170 (2) (2007) 476–489. DOI:10.1016/j.jpowsour.2007.04.018.

[32] P. J. Bugryniec, J. N. Davidson, S. F. Brown, Advanced Abuse modelling of Li-ion Cells – A Novel Description of Cell Pressurisation and Simmering Reactions, Journal of Power Sources 474 (2020) 228396. DOI:10.1016/j.jpowsour.2020.228396.

[33] X. Feng, L. Lu, M. Ouyang, J. Li, X. He, A 3D Thermal Runaway Propagation Model for a Large Format Lithium Ion Battery Module, Energy 115 (2016) 194–208. DOI:https://doi.org/10.1016/j.energy.2016.08.094.

[34] P. T. Coman, S. Rayman, R. E. White, A Lumped Model of Venting During Thermal Tunaway in a Cylindrical Lithium Cobalt Oxide Lithium-ion Cell, Journal of Power Sources 307 (2016) 56–62. DOI:10.1016/j.jpowsour.2015.12.088.

[35] P. Peng, F. Jiang, Thermal Safety of Lithium-ion Batteries with Various Cathode Materials: A Numerical Study, International Journal of Heat and Mass Transfer 103 (2016) 1008–1016. DOI:https://doi.org/10.1016/j.ijheatmasstransfer.2016.07.088.

[36] X. Feng, J. Sun, M. Ouyang, X. He, L. Lu, X. Han, M. Fang, H. Peng, Characterization of Large Format Lithium Ion Battery Exposed to Extremely High Temperature, Journal of Power Sources 272 (2014) 457–467. DOI:https://doi.org/10.1016/j.jpowsour.2014.08.094.

[37] G. Sidebotham, Heat Transfer Modeling An Inductive Approach, Springer Cham, 2015. DOI:10.1007/978-3-319-14514-3.

[38] C. Jin, Y. Sun, H. Wang, Y. Zheng, S. Wang, X. Rui, C. Xu, X. Feng, H. Wang, M. Ouyang, Heating Power and Heating Energy Effect on the Thermal Runaway Propagation Characteristics of Lithium-ion Battery Module: Experiments and Modeling, Applied Energy 312 (2022) 118760. DOI:10.1016/j.apenergy.2022.118760.

[39] A. Kurzawski, L. Gray, L. Torres-Castro, J. Hewson, An Onvestigation into the Effects of State of Charge and Heating Rate on Propagating Thermal Runaway in Li-ion Batteries with Experiments and Simulations, Fire Safety Journal 140 (2023) 103885. DOI:10.1016/j.firesaf.2023.103885.

[40] Y. Liu, L. Zhang, Y. Ding, X. Huang, X. Huang, Effect of Thermal Impact on the Onset and Propagation of Thermal Runaway Over Cylindrical Li-ion Batteries, Renewable Energy 222 (2024) 119910. DOI:10.1016/j.renene.2023.119910.

[41] United Nations, Global Technical Regulation on the Electric Vehicle Safety (EVS) - ECE/TRANS/180/Add.20 (2018).

[42] J. Schöberl, M. Ank, M. Schreiber, N. Wassiliadis, M. Lienkamp, Thermal Runaway Propagation in Automotive Lithium-ion Batteries with NMC-811 and LFP Cathodes: Safety Requirements and Impact on System Integration, eTransportation 19 (2024) 100305. DOI:10.1016/j.etran.2023.100305.

[43] H. Uwitonze, A. Ni, V. M. Nagulapati, H. Kim, H. Lim, CFD Study of Nail Penetration Induced Thermal Runaway Propagation in Lithium-Ion Battery Cell Pack, Applied Thermal Engineering 243 (2024) 122649. DOI:10.1016/j.applthermaleng.2024.122649.

[44] T. L. Bergman, A. S. Lavine, F. P. Incropera, D. P. Dewitt, Fundamentals of Heat and Mass Transfer, 7th Edition, John Wiley & Sons, 2011.

[45] C. Mueller, P. Tsvetkov, A review of heat-pipe modeling and simulation approaches in nuclear systems design and analysis, Annals of Nuclear Energy 160 (2021) 108393. DOI:https://doi.org/10.1016/j.anucene.2021.108393.